NOAA Technical Memorandum GLERL-124

OBSERVATIONS OF THE INTERMEDIATE AND BENTHIC NEPHELOID LAYERS IN SOUTHERN LAKE MICHIGAN DURING THE SUMMER OF 1995

Nathan Hawley
NOAA, Great Lakes Environmental Research Laboratory, Ann Arbor, MI 48105

Great Lakes Environmental Research Laboratory
Ann Arbor, Michigan

August 2003

UNITED STATES
DEPARTMENT OF COMMERCE

Donald Evans
Secretary

NATIONAL OCEANIC AND
ATMOSPHERIC ADMINISTRATION

Conrad C. Lautenbacher, Jr.
Administrator

NOTICE

Mention of a commercial company or product does not constitute an endorsement by the NOAA. Use of information from this publication concerning proprietary products or the tests of such products for publicity or advertising purposes is not authorized. This is GLERL Contribution No. 1276.

This publication is available as a PDF file and can be downloaded from GLERL's web site: www.glerl.noaa.gov. Hard copies can be requested from GLERL, Information Services, 2205 Commonwealth Blvd., Ann Arbor, MI 48105. pubs.glerl@noaa.gov.

ACKNOWLEDGEMENTS

Thanks go the crew of the RV Shenehon and to Andy Winkelman and Chang Hee Lee for their assistance with field operations. The Marine Instrumentation Laboratory of the Great Lakes Environmental Research Laboratory prepared and calibrated the sensors. Mr. Robert Veneklassen of the Muskegon Water Intake facility graciously supplied temperature and turbidity data. Weather data were supplied by Clyde Sweet. Conversations with Gerry Miller and Dave Schwab helped in understanding the properties of internal waves in the lake. Wavelet power spectra software was provided by C. Torrence and G. Compo, and is available at URL: http://paos.colorado.edu/research/wavelets. Software and advice for the wavelet cross coherence calculations was kindly provided by C. Torrence. This work was supported by the Environmental Protection Agency's Lake Michigan Mass Balance Study under interagency agreement DW131671701.

Table of Contents

ABSTRACT 4

1. INTRODUCTION 4
2. SITE DESCRIPTION AND METHODS 5
3. OBSERVATIONS 8
   - 3.1 Vertical Profiles 8
   - 3.2 Time-Series Observations 11
   - 3.3 Wavelet Analysis 16
4. DISCUSSION 26
5. CONCLUSIONS 27
6. REFERENCES 28

Figures

Figure 1. Location map showing the position of the three mooring sites and the water intake station (WI) .. 6
Figure 2 Data from the vertical profiles 9
Figure 3. Observations made at M24 and the Muskegon water intake. 12
Figure 4. Winds and current velocities at M24 and M27 13
Figure 5. Time series measurements at M27 14
figure 6. Power spectra of the observations at M27 15
Figure 7. Scatter plots for the attenuation versus the other parameters measured 35 mab at M27. 17
Figure 8. Time series measurements at M19 18
Figure 9. Current velocities at M19 19
Figure 10. Wavelet power spectra for the parameters measured at 35 mab at M27 21
Figure 11. Wavelet power spectra for the parameters measured at 1 mab at M27 22
Figure 12. A. Wavelet cross coherence for the beam attenuations at 1 and 7 mab at M27 23

Tables

Table 1. Deployment Data 7

Table 2. Thickness of the bnl (m), the total suspended material (g) in a vertical m^2 column extending through the bnl, and the average concentratiaon (g/m3) at M27 and M19 10

Table 3. Periods of high wavelet cross coherence between the 1 mab attenuation and the cross shore velocity at M27, the wavelet energies of the 1 mab attenuation and the 1 mab cross shore velocity, and the phase angle between the two parameters. X indicates that the value is significantly different from zero. A negative phase angle means that the first parameter lags the second. The second, fourth, and fifth episodes occurred during upwelling events 25

Observations of the Intermediate and Benthic Nepheloid Layers in Southern Lake Michigan during the Summer of 1995

Nathan Hawley

ABSTRACT. During the summer of 1995 time series measurements of water transparency, water temperature, and current velocity were made at stations located in 28, 58, and 100 m of water in southern Lake Michigan. Inertial internal waves were the dominant feature of the lake circulation. These waves caused variations in the thickness and in the vertical distribution of suspended sediment in the benthic nepheloid layer. An intermediate nepheloid layer located at the base of the thermocline was also affected by the inertial waves. This layer moves up and down in response to movement of the thermocline due to both inertial waves and to upwelling and downwelling events. Although a direct link between inertial wave action and changes in the benthic nepheloid layer could not be established, the data strongly suggest that the layer is maintained by local resuspension due to a combination of inertial wave action and longer-term processes.

1. INTRODUCTION

Nepheloid layers are a common feature in both large lakes and the world's oceans. The layers are identified by either acoustic (signal strength) or optical measurements (beam attenuation) and are caused primarily by increased concentrations of material suspended in the water column. Benthic nepheloid layers (bnl) are defined as extending upward from the bottom until a minimum attenuation is reached in the middle of the water column (McCave, 1986). Intermediate nepheloid layers (inl, which usually occur at or near pycnoclines) and surface nepheloid layers (snl) have also been identified.

In the oceans benthic nepheloid layers are commonly presumed to be due to local resuspension of bottom sediments, while inls may be formed in several different ways. Cacchione and Drake (1986) suggested that some bnls could be created by the breaking of internal waves on the continental shelf. This hypothesis is supported by both numerical investigations (Ribbe and Holloway, 2001, Wang et al., 2001) that showed that internal waves breaking on the continental shelf could resuspend bottom material, and by observations (Puig et al., 2001) in which a series of increases in bottom turbidity at close to the local inertial period were correlated with increases in the onshore velocity component of the bottom current. Other investigators have found increases in bottom turbidity associated with breaking internal solitons generated by the impingement of long-period internal waves on the continental shelf (Bogucki et al., 1997, Johnson et al., 2001).

In Lake Michigan the bnl is almost always present in the hypolimnion during the stratified period, and is also found to a lesser degree during the unstratified period. Vertical profiles of water temperature and beam attenuation made in the southern basin of the lake in 1983 (Hawley unpublished data) at stations in water depths between 50 m and 150 m show the presence of the bnl at all stations throughout the stratified period. Sandilands and Mudroch (1983) found a similar occurrence of the bnl in Lake Ontario. Profiles made during the unstratified period (Hawley and Lee, 1999, Hawley unpublished data) show that the bnl was far less well developed during the unstratified period except during and immediately after storms. Since internal inertial waves are the dominant feature of the offshore circulation during the stratified period (Mortimer, 1980), and since they do not exist when the lake is unstratified, it seems likely that the formation and maintenance of the bnl is related to the presence of these waves.

The first investigation of the bnl layer in the Great Lakes was by Chambers and Eadie (1981) who speculated that it was caused by local resuspension caused by "the rubbing of the thermocline across the bottom." Since then several subsequent investigators have proposed theories for the origin and maintenance of the bnl in the

Great Lakes. These include local resuspension (Chambers and Eadie, 1981; Sandilands and Mudroch, 1983; Rosa, 1985; Baker and Eisenreich, 1989; Halfman and Johnson, 1989; Mudroch and Mudroch, 1992), downslope advection of nearshore material (Halfman and Johnson, 1989), and settling of biogenic material (Sly, 1994). Although time series measurements of both current velocity and water transparency are required to test these hypotheses, none were made in any of these studies.

Recently however the results of several such time series studies have been reported. Hawley and Lesht (1995) analyzed several months of time series observations in Lake Michigan in water depths of 65-100 m and found no instances of bottom resuspension. They suggested that the bnl was maintained by a combination of vertical mixing and the offshore transport of material during downwelling events. Although Hawley and Lesht speculated that internal wave action supplied at least some of the energy for vertical mixing, their data was insufficient to document their speculation. Hawley and Murthy (1995) found no evidence of either resuspension or downslope transport during a downwelling event in Lake Ontario. Lee and Hawley (1998) examined the effects of upwelling and downwelling events on the bnl in Lake Michigan. They too found that material was not directly supplied to the bnl during downwelling events. Although inertial internal waves are evident in the initial part of their observations, they did not discuss their effects. In all of these studies variations in both the thickness of the bnl and the concentration of material suspended within it were observed, but no obvious physical forcing was identified.

More recently Hawley and Muzzi (2003) described changes in turbidity and temperature recorded by a moored vertical profiler. They found that changes in the depth of the inl coincided with changes in thermocline depth due to both upwelling and downwelling events and to inertial internal waves. They also observed changes in the bnl due to inertial waves and found that episodes of high bottom turbidity coincided with periods when the thermocline was elevated. Hawley and Muzzi determined that the total amount of material suspended in the bnl changed with time and (although no velocity measurements were made) speculated that the high turbidity episodes were caused either directly or indirectly by the shoaling of inertial internal waves on the lake slope. This paper examines time series observations of temperature, current velocity, and water transparency made during the summer of 1995 just prior to the observations reported by Lee and Hawley (1998). No obvious local resuspension events were observed during the observation period, but substantial changes in both the thickness of the bnl and the concentration of suspended material occurred. The analysis presented here attempts to determine the physical processes responsible for the maintenance of the inl and bnl in Lake Michigan.

2. SITE DESCRIPTION AND METHODS

Instrumented tripods were deployed at three stations in southern Lake Michigan during the summer of 1995 as part of the Environmental Protection Agency's (EPA) Lake Michigan Mass Balance Program. The stations were located in water depths of 28 m (M24, 5 km offshore), 58 m (M27, 10 km offshore), and 100 m (M19, 28 km offshore) along a transect that originated in Muskegon, Michigan and ran roughly perpendicular to the shoreline (Figure 1). M27 is one of the sites described by Lee and Hawley (1998), and is located very close to the site where Hawley and Muzzi (2003) made their observations. Bottom contours in this area (which is near the northern edge of the southern basin of the lake) run roughly parallel to the shoreline, which is oriented northwest to southeast. Depth soundings along the transect show a relatively flat surface to about 30 m, then a steeper slope extending to about 80 m before the relatively flat lake bottom is reached.

Boyce et al. (1989) reviewed the seasonal thermal cycle of the Great Lakes and described the various physical processes that occur. Circulation in the lake is driven by the wind, but (because of Lake Michigan's size) rotational forces are important. The lake is stratified from June to November, with a warm epilimnion separated from the colder hypolimnion water (temperature near 4°C) by a thermocline 10-20 m thick. A two-layer circulation system is set up, with the epilimnion responding directly to the wind stress. This causes upwelling and downwelling events to occur in the coastal boundary layer, which is about 10 km wide (Murthy and Dunbar, 1981). On the eastern side of Lake Michigan winds to the north cause downwelling of surface waters while winds

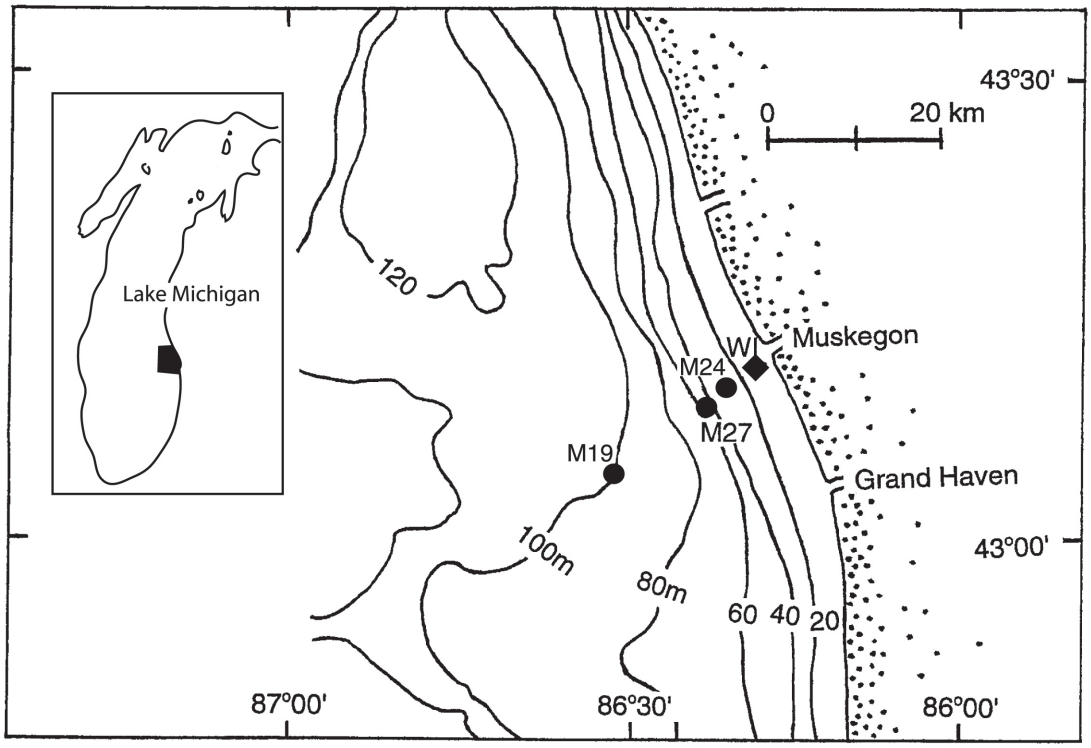

Figure 1. Location map showing the position of the three mooring sites and the water intake station (WI).

to the south induce upwelling of colder bottom water. These disturbances may then propagate counter-clockwise around the lake as internal Kelvin waves (Mortimer, 1980; Boyce et al., 1989). The amplitude of these waves decays with distance from shore, so their effects are seen only within a few km of the shoreline. We would expect to see Kelvin wave effects at M24, but not at M27 or M19.

Farther offshore the winds generate (quasi-)standing internal Poincaré waves. Since these waves have periods at or slightly less than the local inertial period (about 17.6 h for Lake Michigan), they are called near-inertial waves. These internal waves occur in both the epilimnion and the hypolimnion throughout the stratified period. The horizontal currents associated with these waves move in a clockwise direction; the horizontal trajectories of the water particles are nearly circular with a radius of about one km (Mortimer, 1980). The effects of the waves can also be seen in temperature records since the thermocline depth at a given point varies with the phase of the wave. However since the motion at any given point may be the result of a combination of waves with different modes, and since the maximum currents and maximum temperature differences occur at different locations, it is unlikely that any consistent relationship between the temperatures and currents will occur.

Details of the deployments are given in Table 1. Each of the three tripods included a data acquisition system, a power supply, and an array of sensors that made temperature and water transparency measurements at 0.9, 7, and 17 meters above the bottom (mab). The bottom sensors were attached directly to the tripods while the sensors at the upper elevations were attached to a mooring wire that was attached to a surface float. Additional measurements were made at M27 (35 mab) and M19 (35 and 65 mab) with separate packages attached to the mooring wire. All of the sensors were sampled at 1 Hz for 1 minute every hour; the averaged values and their standard deviations were then recorded.

Temperature measurements were made using Yellow Springs thermistors accurate to 0.2° C. Water transparency measurements were made using Sea Tech transmissometers (25-cm pathlength) and Sea Tech light-scattering sensors (LSS). The transmissometer and light-scattering sensor readings were recorded to the nearest 0.001 volt over a nominal 5-volt scale. When converted to beam attenuation, this is equivalent to a precision of about 0.005 1/m. Although the readings of both the transmissometers and the LSS respond to changes in the suspended sediment concentration, we found that each LSS responded differently when compared to the beam attenuation

Table 1. Deployment Data.

Station	Water intake	M24	M27	M19
Deployed	-	July 11, 1995	July 11, 1995	July 12, 1995
Retrieved	-	August 22, 1995	August 22, 1995	August 21, 1995
Latitude	43° 12.30' N	43° 11.39' N	43° 10.14' N	43° 03.66' N
Longitude	86° 20.83' W	86° 22.67' W	86° 26.02' W	86° 37.81' W
Water depth (m)	13 m	28 m	58 m	100 m
VACM Current Measurements				
Height (mab)	-	1,17	1,17,35	1,17,35,65
Sampling rate	-	15 min ave	15 min ave	15 min ave
Sampling per.	-	continuous	continuous	continuous
Temperature Measurements				
Height (mab)	3	0.9,7,17	0.9,7,17,35	0.9,7,17,35,65
Sampling rate	Hourly	1 Hz	1 Hz	1 Hz
Sampling per.	Single meas.	1 minute/hour	1 minute/hour	1 minute/hour
Transparency Measurements				
Height (mab)	3	0.9,7,17	0.9,7,17,35	0.9,7,17,35,65
Sampling rate	Bi-hourly	1 Hz	1 Hz	1 Hz
Sampling per.	Single meas.	1 minute/hour	1 minute/hour	1 minute/hour
Size Analysis				
Percent sand	100%	94%	55%	40%
Percent silt	0%	5%	42%	44%
Percent clay	0%	1%	3%	16%
Mean dia. (mm)	0.26	0.24	0.16	0.14

coefficient (bac, which is independent of the instrument used) computed from the transmissometer readings. Bottom material from M27 was used to perform a five-point calibration between the voltage reading for each LSS and the bac measured by a transmissometer. These data were then used to construct a separate correction equation for each of the LSS sensors. The correction equations varied significantly from sensor to sensor, but the r^2 values were all greater than 0.99. Hawley and Zyren (1990) found a linear relationship between bac and the concentration of suspended material in southern Lake Michigan, so in this paper we use bac as a surrogate for suspended particulate material.

Currents were measured with EG&G vector-averaging current meters (VACM) deployed on separate moorings near the tripods. These moorings were deployed on 26 May and retrieved on 12 October, and had meters located at 1, 17, 35 (at M27 and M19), and 65 (at M19 only) mab. The VACMs have a lower threshold of 0.02 m/s, an accuracy of 0.01 m/s, and record a continuous 15-minute average. Several of the near-bottom VACMs stalled one or more times during the deployment when the speed decreased below the threshold. Currents were rotated 37° to provide the alongshore and cross-shore velocity components.

Temperature and water turbidity observations were also made at the Muskegon Municipal Water Intake (WI in Figure 1). The water intake is located 3 mab approximately 1.5 km offshore in 13 m of water. Temperature

was measured hourly, but because turbidity was measured every other hour an averaged value between each two measurements was used to create an hourly record. The turbidity readings were reported in Nephelometric Turbidity Units (NTU). These were converted to BAC by determining the BAC at 5 NTU values and constructing a correction equation. These measurements were made using the same standard turbidity solution used to calibrate the water intake's turbidity meter. Because a time lag of up to 6 hours could exist between the time the water entered the intake and the time that the measurements were made at the station on shore, the intake records were shifted 6 hours prior to plotting. However since the time lag is not constant, the intake data are not always simultaneous with the other measurements.

During the deployment period vertical profiles of water temperature and bac were made 13 times at the three stations and 9 times at three other stations (located in 12, 45, and 80 m of water) with a Seabird CTD unit equipped with a 25-cm Sea Tech transmissometer. Additional profiles were made at the stations at irregular intervals between April and November. Hourly wind data were obtained from a weather station located at the entrance to Muskegon Harbor. These observations were used as input to the GLERL-Donelan wave model (Schwab et al., 1981) to calculate the surface wave height and period.

Bottom sediment samples were collected with a Ponar bottom grab sampler at the water intake station and at the mooring sites. Examination of these samples showed that the bottom material was cohesive at M27 and M19 and noncohesive at M24 and the water intake. The material from the top centimeter was wet sieved to separate the sand fraction (diameter > 0.064 cm) prior to determining the fine-sediment size distribution with a Spectrex model ILI-1000 laser particle counter. The sizes of the coarser material were analyzed with a settling tube. The analyses show that the bulk (over 70%) of the coarser material at all of the stations was medium and fine sand (diameters between 0.5 and 0.125 mm). Results from the size analyses are included in Table 1. Observations made with a remotely operated vehicle show that the bottom is flat (no bedforms) at stations M24, M27, and M19, and rippled at the water intake station.

Spectral time series analyses were done using standard techniques. The wavelet power spectra were computed using software developed by Torrence and Compo (1998), the wavelet cross coherences were calculated using the algorithm presented by Torrence and Webster (1999). Values were calculated each hour at 37 periods ranging from 2.2 h to 325 h. The interval between the periods varied logarithmically and was about 2.2 h at 17.6 h. The 95% confidence level for the spectral coherence was calculated using the method of Jenkins and Watts (1969). The confidence levels for the wavelet cross coherences and phase angles are based on Monte Carlo simulations (20,000 simulations).

3. OBSERVATIONS

3.1. Vertical Profiles

The vertical profiles at M24 (Figure 2) show that the thermocline intersected the bottom until July 26; after that time the increasing stratification (the temperature in the epilimnion increased from 20° to 24°C during the deployment) moved the thermocline higher in the water column. The bnl was either very thin or absent until late in the deployment, and the concentration of suspended material was low compared to that at the deeper sites. The horizontal lines in Figure 2 show the elevations at which the time series measurements were made. The sensors 7 meters above the bottom (mab) were located in either the thermocline (defined as the region between 10 and 20°C) or the hypolimnion, while the 17 mab sensors were in the epilimnion (except at the very end of the deployment), and the 1 mab sensors were in the hypolimnion.

At M27 the profiles show that as the lake became more stratified the depth of the thermocline (determined as the depth of the 10° isotherm) decreased from about 23 m to 12 m. This decrease was not monotonic however, and the thermocline depth could vary several meters in one day (July 12-13). The sensors located 1, 7 and 17 mab were always located in the hypolimnion, but the sensors 35 mab were sometimes in the thermocline. The beam attenuation measurements show a well-developed bnl in each of the profiles. The thickness of the bnl varied

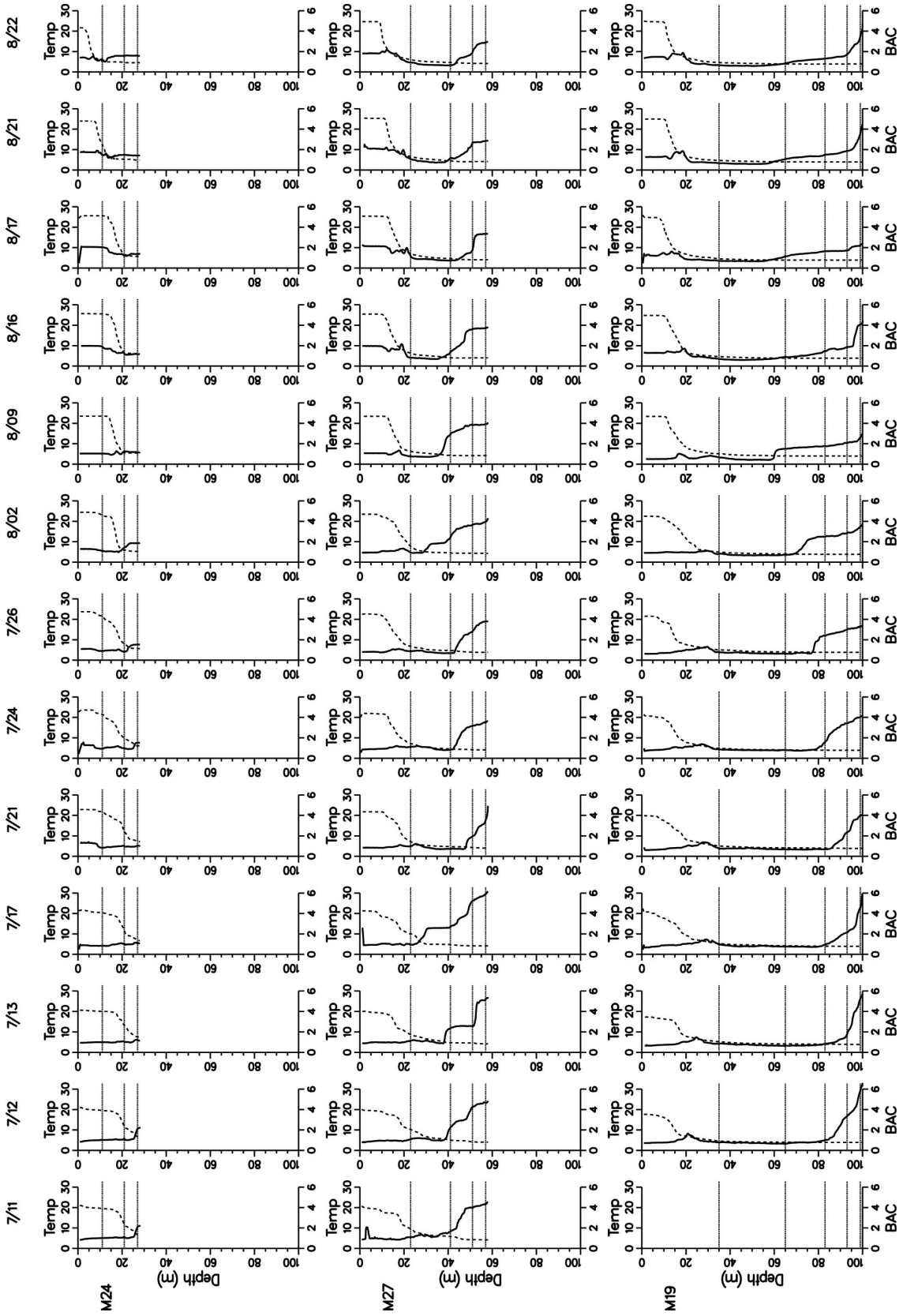

Figure 2. Data from the vertical profiles. The solid line is the bac (1/m), and the dashed line is the temperature (degrees C). The top row shows profiles made at M24, the middle row the profiles made at M27, and the bottom row the profiles made at M19. Heights of the time series observations are shown by the horizontal lines. No profile was made at M19 on July 11.

Table 2. Thickness of the bnl (m), the total suspended material (g) in a vertical m^2 column extending through the bnl, and the average concentration (g/m^3) at M27 and M19.

Date	M27 BNL Thickness	M27 Total Material	M27 Average Concentration	M19 BNL Thickness	M19 Total Material	M19 Average Concentration
July 11	26	134	5.4	-	-	-
July 12	22	140	6.4	35	122	3.5
July 13	22	128	5.8	28	81	2.9
July 17	39	244	6.3	24	85	3.5
July 21	12	49	4.1	26	79	3.0
July 24	21	91	4.3	28	124	4.4
July 26	20	87	4.4	25	120	4.8
August 2	35	160	4.6	39	154	3.9
August 9	29	146	5.0	43	131	3.0
August 16	21	110	5.2	55	120	2.2
August 17	22	65	3.0	48	113	2.4
August 21	24	73	3.0	46	121	2.6
August 22	19	58	3.1	50	111	2.2

considerably - on some days it occupied the entire hypolimnion (on July 17 for instance) while on other days it was confined to a fairly thin layer near the bottom (July 21). The bac decreased with increasing height above the bottom, but the shape of the profile varied from day to day. On a few days a stepped structure occurred (July 13 and July 21) while on other days the profile was much smoother. The maximum attenuation in the bnl varied between 3 and 6 1/m, while the minimum attenuation above the bnl was approximately 0.65 1/m. The minimum value in each profile was used to determine the thickness of the bnl on that day. The attenuation measurements in the bnl were converted to the concentration of suspended material using the equation of Hawley and Zyren (1990). Table 2 shows the thickness of the bnl, the amount of suspended material in a m^2 column extending through the bnl, and the average concentration of material in the bnl. These calculations show that both the thickness of the bnl and the amount of material suspended within it could vary by more than a factor of 2 within a few days.

Many of the profiles also show an inl near the base of the thermocline. This layer is most noticeable at the end of the deployment. The observations at 35 mab were usually made in the clearer water between the bnl and the inl, while the observations made at the lower elevations were usually made within the bnl. However on several occasions the 17 mab observations were made either above or very near the top of the bnl, and on July 17 the 35 mab observations were within the bnl.

At M19 all of the sensors were always located in the hypolimnion well below the inl. As stratification increased, the depth of both the thermocline and the inl decreased. The bnl is well-developed at this site throughout the deployment. Since the thickness of the bnl is greater than at M27, the amount of material in suspension is comparable to that at M27 even though the average concentration is usually lower (Table 2). However near bottom attenuations at M19 often were equal to or greater than those observed at M27. As at M27 both the thickness of the bnl and the concentration of suspended material could vary considerably within a few days.

Profiles were also made at stations in 12 m, 45 m, and 80 m of water on 9 occasions (not shown). The bnl was never observed at the 12 m station even though the water was stratified at the end of the deployment, but was always present at the two deeper stations. At the 80 m station the bnl frequently resembled that at M19, with near bottom concentrations higher than at M27, while the bnl at the 45 m station was similar to that at M27.

3.2. Time Series Observations

Winds during the deployment were light (less than 10 m/s) and varied in direction (Figure 3). The light winds produced relatively small waves during the deployment - maximum wave heights and periods recorded by NDBO buoy 45007 (located in the center of the southern basin about 70 km away, Figure 1) were about 2 m and 6.5 s. Wave parameters at the study site (calculated using the GLERL-Donelan wave model, Schwab et al. 1981) are somewhat larger than those at the buoy. No current velocity measurements were made at the water intake, but the maximum bottom stress due to wave action alone (calculated from the wave model results using the method of Li and Amo,s 2001) was about 0.25 Pascals. Although this value is slightly greater than that needed to erode the material at this site (0.20 Pascals, calculated using the Li and Amos method), no resuspension was observed at the water intake. The maximum bottom stress due to the combined effects of waves and currents at M24 was 0.06 Pascals, but no resuspension was observed at this site either (the critical value for erosion at this site is 0.17 Pascals). At M27 the effects of waves at the bottom were negligible, but the maximum stress due to the currents alone was 0.07 Pascals. This value is also considerably below the threshold required for sediment movement (0.13 Pascals). At M19 the maximum current stress was also significantly lower than that needed to erode the bottom material.

Winds were predominantly to the north, so downwelling conditions prevailed during most of the deployment, but the southward winds on July 18, August 1, and at the end of the deployment produced upwelling events. The temperature records at the water intake and at M24 show that upwellings occurred on July 18-19, August 1-4, and August 20-24. Another upwelling occurred on August 6-10 although there was no obvious wind event to cause it. The first three of these upwellings produced increases in the concentration of suspended material at M24 but not at the water intake. Similar increases were previously described by Lee and Hawley (1998) and appear to be a common consequence of upwellings at this site. It is not clear what caused the increase in bac at the water intake between August 14 and August 20, but it does not appear to be due to surface wave action. The 17 mab currents at M24 (Figure 4) are usually a direct consequence of the imposed wind stress except during the upwellng events when the rotary motion due to Poincaré waves is apparent. The currents at 1 mab show little evidence of these waves. Currents at 1 mab are very slow and directed primarily alongshore with an offshore component. Power spectra analyses of the parameters show a peak at the inertial period (17.6 h) for most of the parameters at M24 and for the water temperature at the water intake.

Currents at the three elevations at M27 (Figure 4) were quite similar to each other although the rotary motions due to the near-inertial internal waves are more pronounced at the upper elevations. The rotary motions dominate the circulation on July 17-22 and are also important between July 28 and August 12. These intervals are probably the result of the modification of the long-term currents by the upwelling events that occurred, although the reason for the low currents between July 28 and August 1 is unclear. These two intervals divide the current record into 5 parts, with relatively strong alongshore flow during the other three periods (July 11-17, July 22-28, and August 12-22). This alongshore motion is much more pronounced than at either M24 or M19. The currents show a net transport to the south until August 12, and northward after that. The cross shore transport is considerably less than the alongshore movement; the net transport was offshore prior to August 12, and onshore afterward.

The most noticeable feature of the time series measurements at M27 (Figure 5) are the numerous short-period oscillations in the records. These oscillations are much more prevalent than at the shallower stations. Power spectra analyses (Figure 6) show peaks in the energy spectrum at the inertial period for all of the parameters except the 1 mab attenuation, so the short-period oscillations are probably due to the passage of inertial waves. The effects of the upwellings are evident in the decreases in the 35 mab temperature on July 18 and August 1. Temperatures at the other three elevations are much lower and show little change throughout the deployment.

The attenuation measurements show no obvious resuspension events, but there is considerable variation at both the inertial period and on a longer time scale. The long term variations in the attenuations at the two lowest elevations are very similar to each other. Both have their highest values (July 18 and August 5) during intervals when the currents were weak, and show a gradual decline after August 12. The 17 mab observations are similar to those

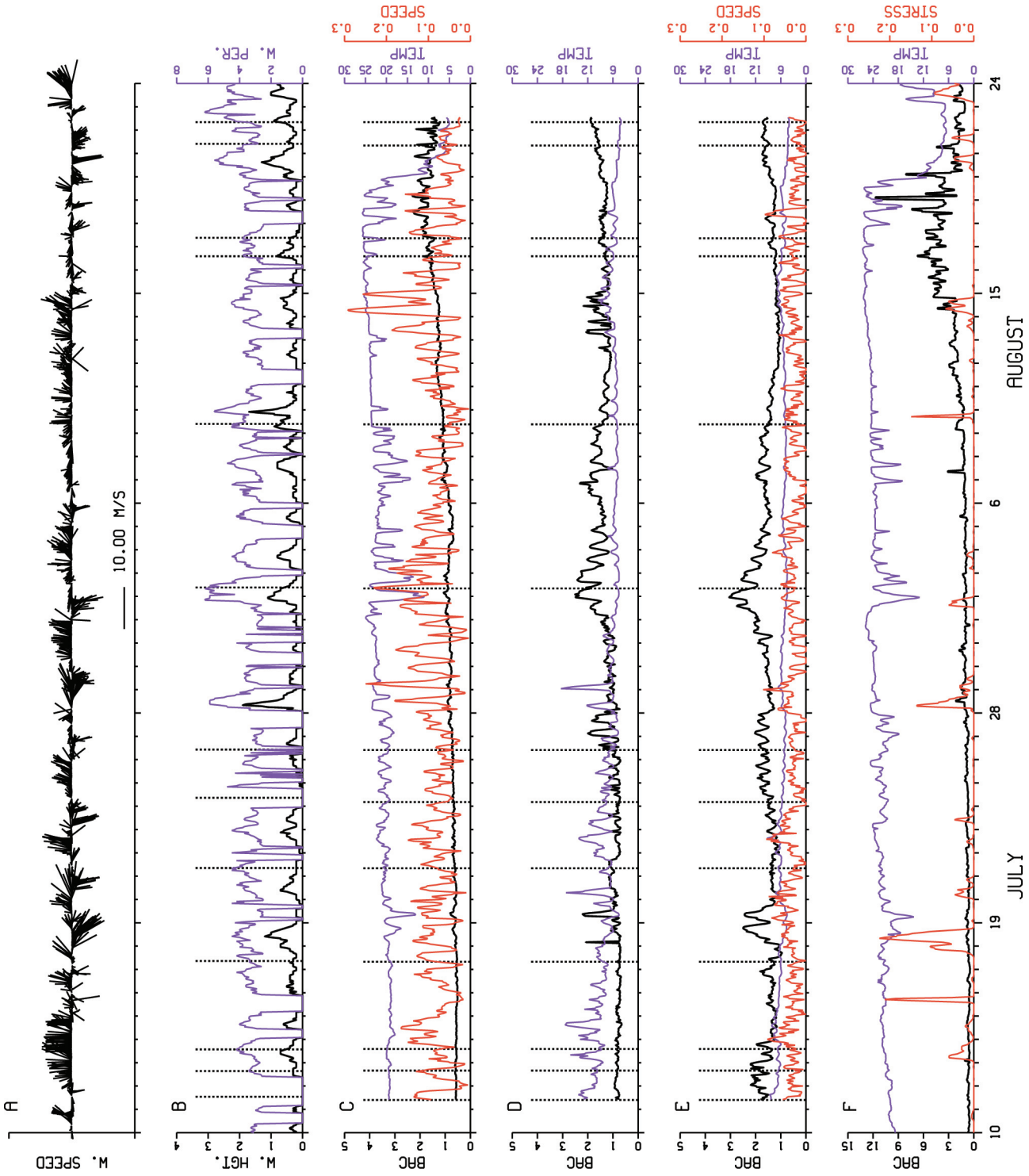

Figure 3. Observations made at M24 and the Muskegon water intake. The colors of the axes correspond to the colors of the observations. The dotted vertical lines indicate the times of the profiles shown in Fig. 2. **A.** The wind velocity at Muskegon. **B.** The significant wave height (black, m) and the peak-energy wave period (blue, s) calculated by the GLERL wave model. **C.** The beam attenuation (black, 1/m), temperature (blue, degrees C), and current speed (red, m/s) 17 mab at M24. **D.** The beam attenuation (black, 1/m), temperature (blue, degrees C at 7 mab at M24. No current measurements were made at this elevation. **E.** The beam attenuation (black, 1/m), temperature (blue, degrees C), and current speed (red, m/s) 1 mab at M24. **F.** The beam attenuation (black, 1/m), temperature (blue, degrees C), and the bottom stress due to wave action calculated from the wave model parameters (red, Pascals) at the water intake.

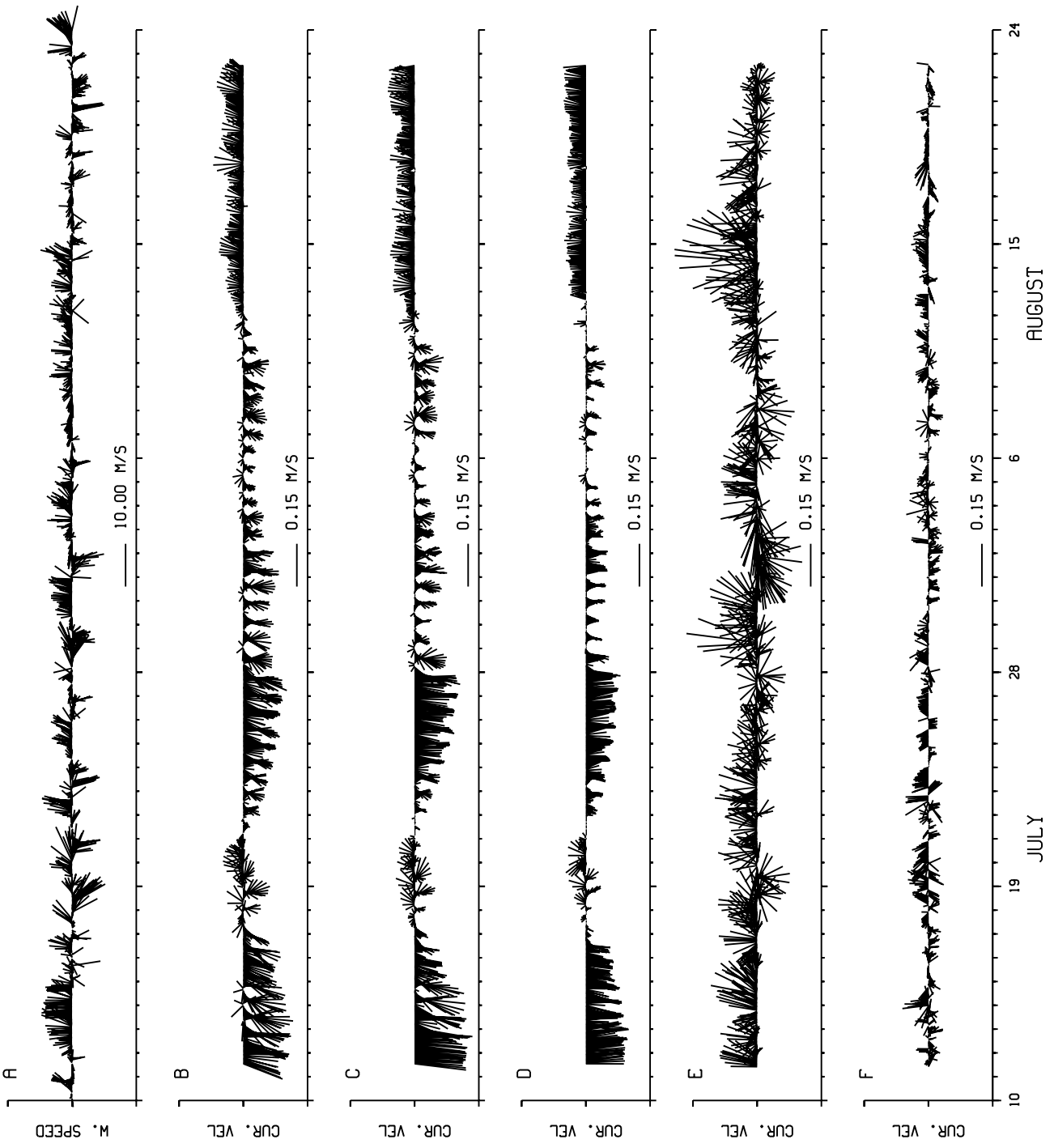

Figure 4. Winds and current velocities at M24 and M27. The currents have been rotated 37° so that up (north) and down (south) are alongshore and offshore is to the left. **A.** Wind speed at Muskegon. **B.** Current velocity 35 mab at M27. **C.** Current velocity 17 mab at M27. **D.** Current velocity 1 mab at M27. **E.** Current velocity 17 mab at M24. **F.** Current velocity 1 mab at M24.

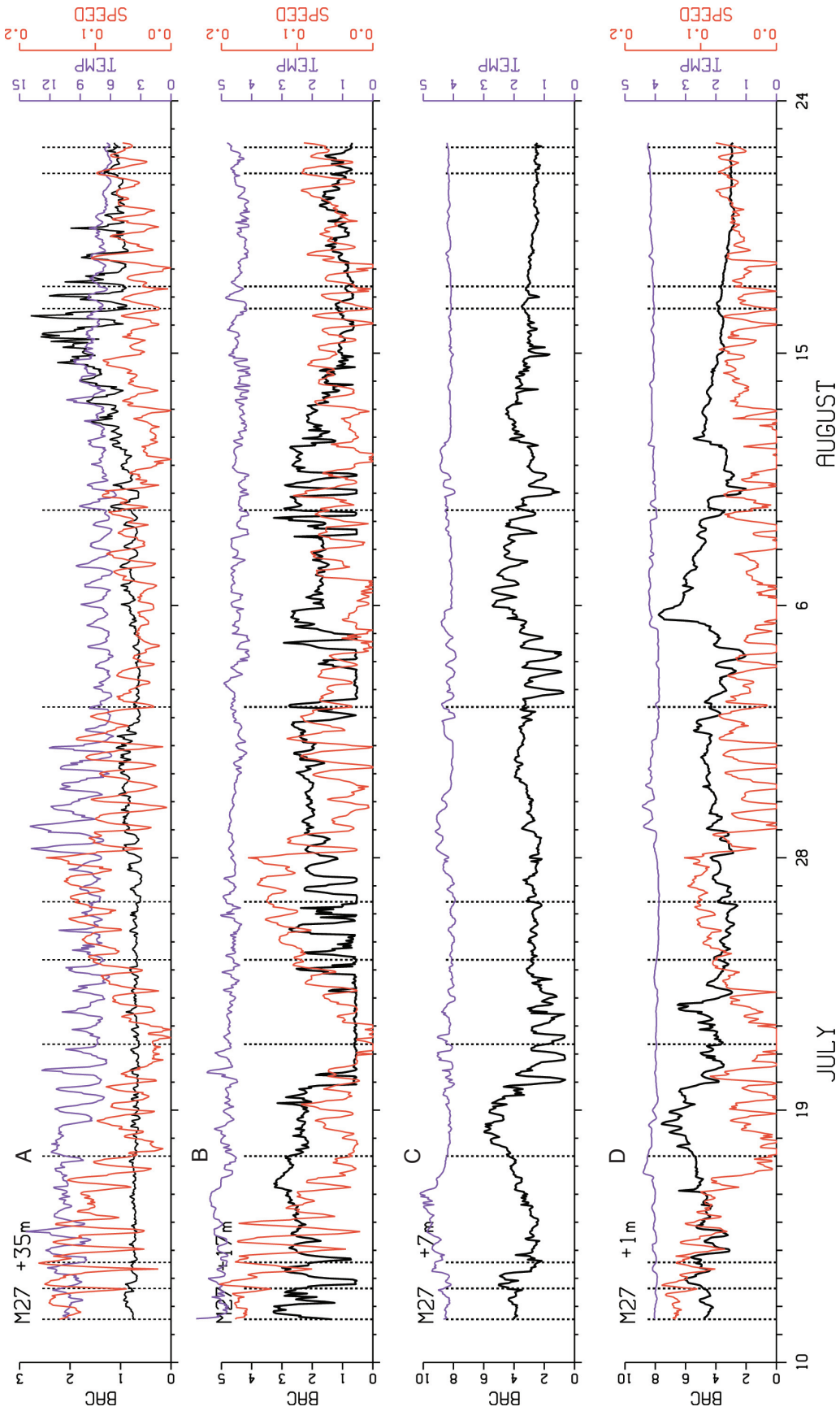

Figure 5. Time series measurements at M27. The colors of the axes correspond to the colors of the observations. The dotted vertical lines indicate the times of the vertical profiles shown in Fig. 2. **A.** The beam attenuation (black, 1/m), temperature (blue, degrees C), and current speed (red, m/s) 35 mab. **B.** The beam attenuation (black, 1/m), temperature (blue, degrees C), and current speed (red, m/s) 17 mab. **C.** The beam attenuation (black, 1/m), temperature (blue, degrees C at 7 mab. No current measurements were made at this elevation. **D.** The beam attenuation (black, 1/m), temperature (blue, degrees C), and current speed (red, m/s) 1 mab.

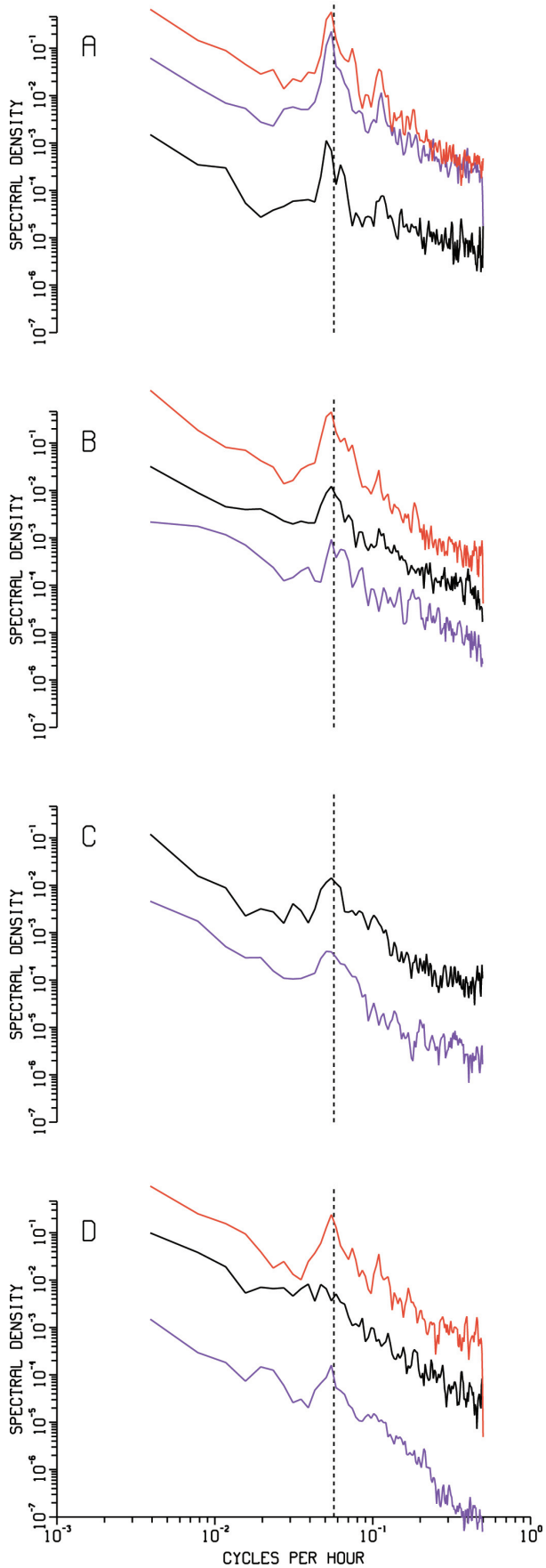

Figure 6. Power spectra of the observations at M27. The black lines are the beam attenuations, the blue lines the temperatures, and the red lines are the current speeds. The dashed vertical line is the inertial period (17.6 h). **A.** 35 mab. **B.** 17 mab. **C.** 7 mab. No current measurements were made at this elevation. **D.** 1 mab.

at the lower elevations, but there are two intervals (July 20-23 and August 3-4) when the attenuation is both very low and relatively constant. These are periods when the thickness of the bnl was less than the elevation of the sensor. The vertical profile made on July 21 confirms that the bnl was only 12 m thick on that day. Immediately before and after these intervals the attenuation varied greatly; these are periods when the top of the bnl oscillated up and down past the sensor. At other times during the deployment (July 14-20, July 28- August 2, August 5-8, and August 12-23) the bnl was over 17 m thick. The top of the bnl moved up and down past the 7 mab sensor on July 20-23 and August 3-4, so the thickness of the bnl varied from less than 7 m to over 35 m (on July 17) during the observation period. The variations in the 35 mab attenuation are much less than at the lower elevations and show little relationship to them. The 35 mab attenuation reaches its highest values near the end of the deployment, when the attenuations at the other three elevations are decreasing.

Scatter plots show that the current velocity components at the different depths are very similar to each other, but this is not true for either the temperatures or the attenuations. Nor is there any consistent relationship between the attenuation and the other parameters at a given depth (Figure 7). Correlation coefficients based on linear regressions for different pairs of parameters show that the current speeds and velocity components at different elevations are highly correlated, but there is little correlation between either the temperatures or the attenuations at different elevations, or between the attenuation and any of the other parameters at a given depth. The spectral coherences between the same parameter at different elevations are somewhat higher than the correlation coefficients, but they are only significantly different from zero for the current speeds and the velocity components, and between the near-bottom (1 and 7 mab) temperatures. Nor are the coherences between the beam attenuation and the other parameters at the same depth significantly different from zero.

No evidence of upwelling or downwelling events were observed at M19 (Figure 8), and the currents at all elevations are dominated by inertial waves (Figure 9). Power spectra analyses of the observations show large peaks at the inertial period for all of the currents and temperatures and for the 65 mab bac. There is little net transport at this station in any direction. The temperature variations are small due to the depths at which the observations were made, but the bacs show that the bnl increased in thickness during the deployment, and there are intervals at 7, 17, and 35 mab during which the top of the bnl moved up and down past the sensors. The fact that the bnl behaves similarly to that at M27 even though no indication of upwelling or downwelling activity is evident suggests that the primary cause of changes in the bnl is inertial waves, but exactly how the waves affect the nepheloid layers is unclear. An inl is apparent in the vertical profiles, but since the uppermost time series sensors (65 mab) were well below the inl, there is little indication of its movement in the time series observations.

3.3. Wavelet Analysis

Nepheloid layers are well developed at the three stations and occur at these stations throughout the stratified period (the layers are present in all vertical profiles made between the time stratification began in early May and ended in late October). This indicates that conditions during the stratified period are favorable in some way for the development and maintenance of these layers. The peaks in the power spectra suggests that inertial wave action is somehow related to the occurrence of the layers, but the analysis so far shows no significant correlation between inertial motions in either the currents or the water temperature and changes in bac. However in order for the correlation coefficients to be large, or for the coherences to be significantly different from zero, the relationship between the parameters must be both linear and relatively constant with time. Since the scatter plots between bac and the other parameters show that neither of these conditions hold, it is not surprising that the correlations and the coherences are low. It would be more useful to identify periods within the observation period when the relationship between the various parameter pairs is relatively constant, and then determine the relationship during those intervals.

Wavelet analysis is a relatively recent development in time series analysis that facilitates such an approach. Its chief advantage over Fourier analysis is that it allows one to characterize the energy distribution of a parameter as a function of both time and period (or frequency). Since the analysis is sensitive to changes in the observed parameters it is highly suitable for the analysis of events that occur during only a small fraction of the observation

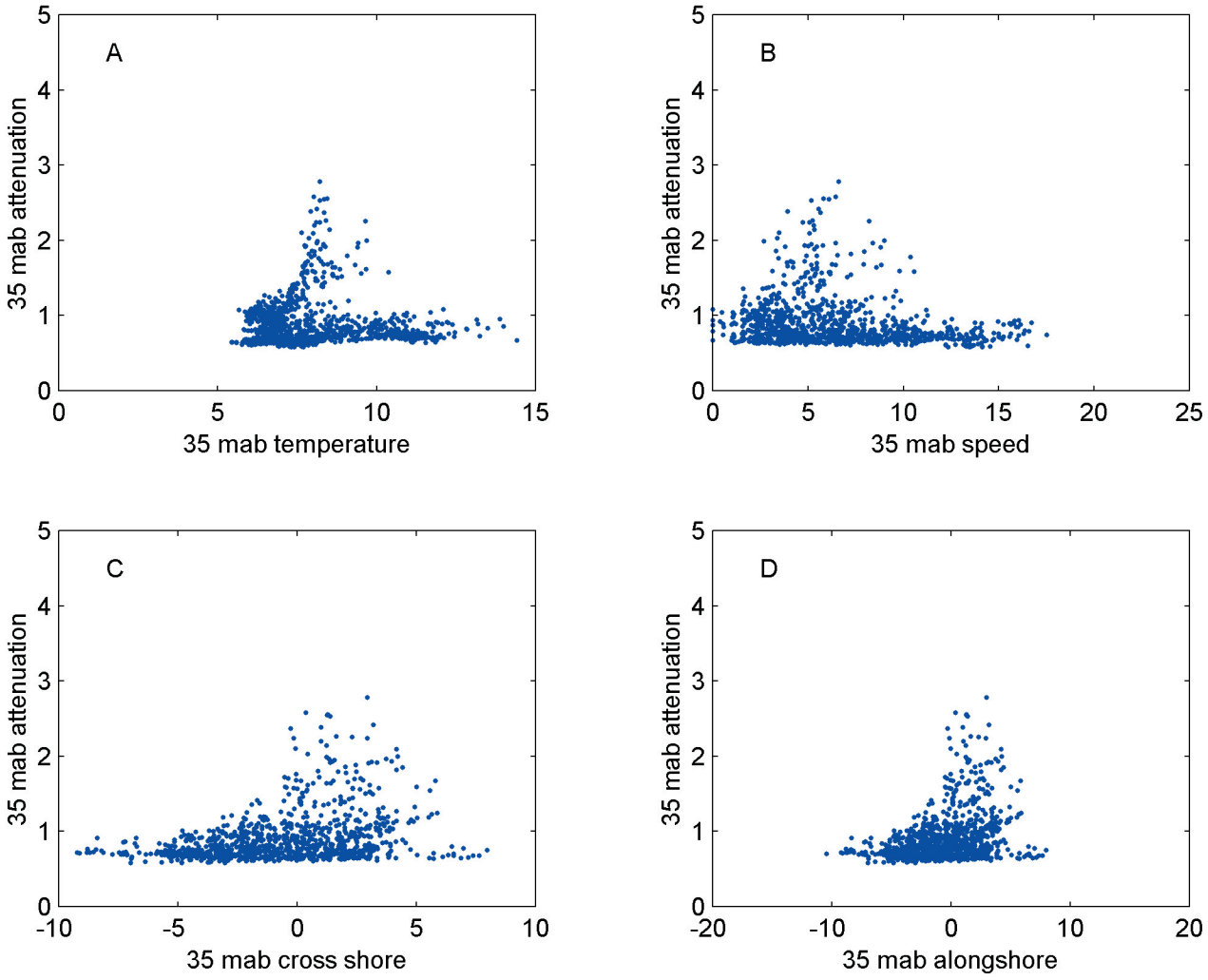

Figure 7. Scatter plots for the attenuation versus the other parameters measured 35 mab at M27. **A.** Temperature and attenuation. **B.** Speed and attenuation. **C.** Cross shore velocity and attenuation. **D.** Alongshore velocity and attenuation.

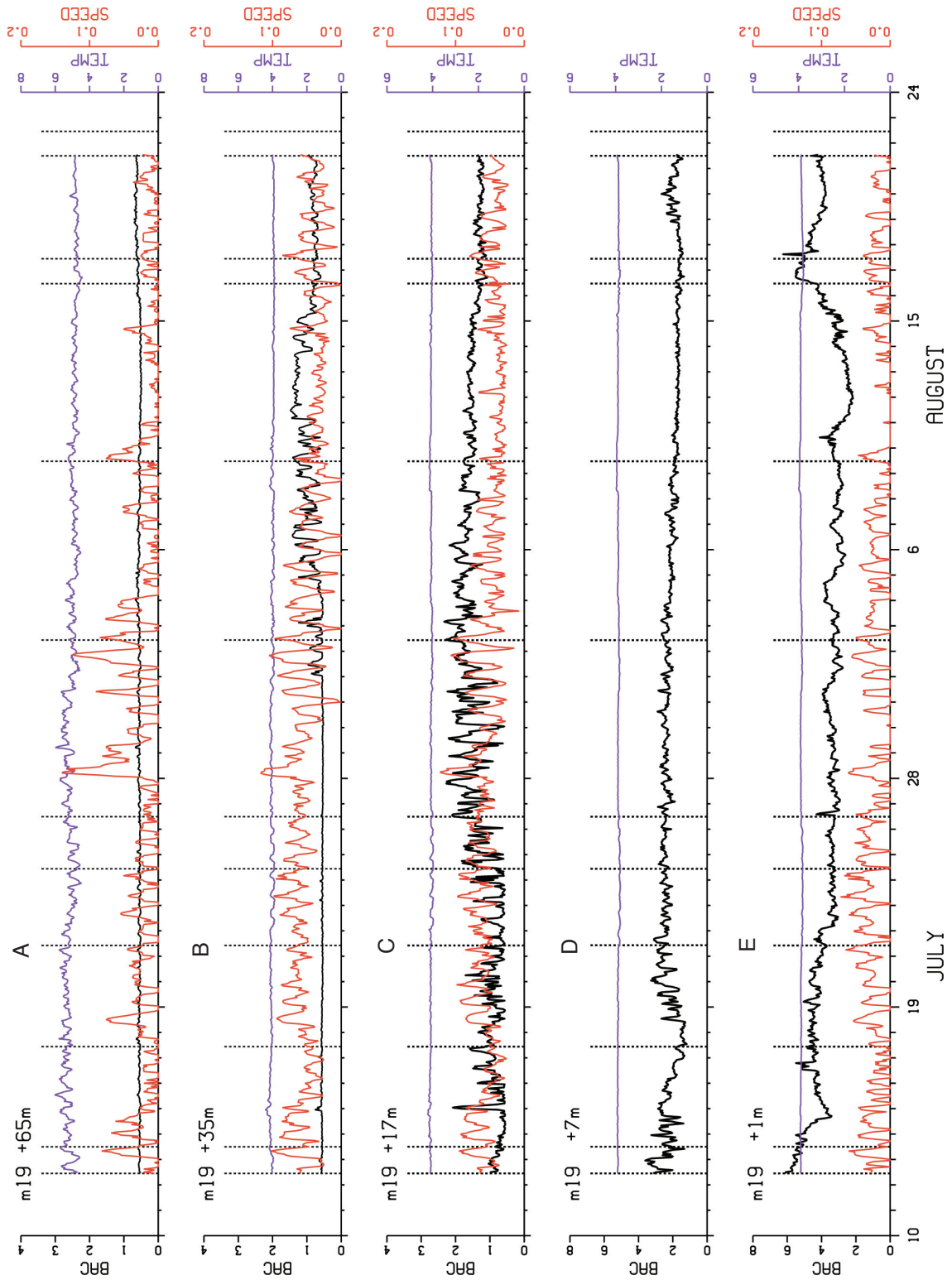

Figure 8. Time series measurements at M19. The colors of the axes correspond to the colors of the observations. The dotted vertical lines indicate the times of the vertical profiles shown in Fig. 2. **A.** The beam attenuation (black, 1/m), temperature (blue, degrees C), and current speed (red, m/s) 65 mab. **B.** The beam attenuation (black, 1/m), temperature (blue, degrees C), and current speed (red, m/s) 35 mab. **C.** The beam attenuation (black, 1/m), temperature (blue, degrees C), and current speed (red, m/s) 17 mab. **D.** The beam attenuation (black, 1/m), temperature (blue, degrees at 7 mab. No current measurements were made at this elevation. **E.** The beam attenuation (black, 1/m), temperature (blue, degrees C), and current speed (red, m/s) 1 mab.

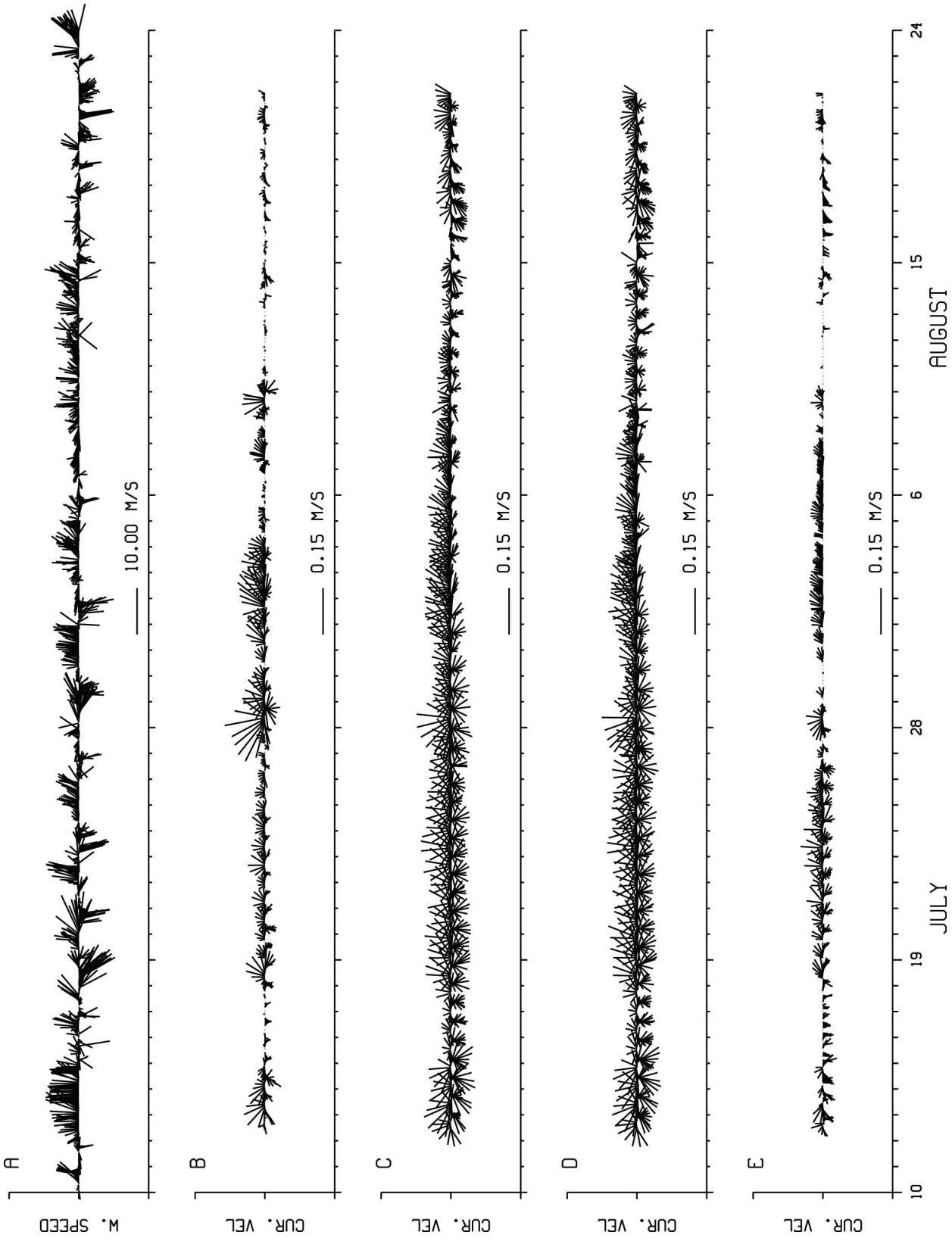

Figure 9. Current velocities at M19. The currents have been rotated 37° so that up (north) and down (south) are alongshore and offshore is to the left. **A.** Current velocity 65 mab. **B.** Current velocity 35 mab. **C.** Current velocity 17 mab. **D.** Current velocity 1 mab.

period. The Morlet wavelet is used here – this wavelet has been used in several previous environmental studies (Meyers et al., 1993, Liu and Miller, 1996, Torrence and Webster, 1999) because it is relatively easy to interpret, and because it offers fairly good resolution in both time and period. The analysis below uses wavelets to identify intervals in the records when inertial wave action was most pronounced, and to determine if a consistent relationship exists during these intervals between the attenuation and the other parameters. The analysis concentrates on the observations at M27 since the bacs vary most at this station.

Figures 10 and 11 show the wavelet power spectra for some of the observed parameters at M27 as a function of period (in hours) and time. The contours are multiples of the energy level that is significantly different from zero at the 95% confidence level when compared to a white noise spectra (Torrence and Compo, 1998). The energy in most of the wavelet power spectra is concentrated in two distinct bands: one at periods greater than about 100 hours and the second centered around the inertial period. This concentration is most obvious in the velocities, but can be seen in the other parameters as well. Significant energy at the inertial period is most continuous over time in the velocities - particularly the cross-shore component - and is also more continuous at the upper elevations. The distribution over time of the longer-period energy is somewhat misleading since edge effects affect the values of the wavelet coefficients at the beginning and end of the observation interval. This effect is significant over about two times the period for which the wavelet coefficients are calculated (the cone of influence, Weng and Lau, 1994), so although the general observation that there is considerable energy at the longer periods is undoubtedly correct, it would be risky to say too much about the distribution of energy with time for periods greater than 100 h.

A comparison of the wavelet spectra to the 35 mab attenuation measurements shown in Figure 6 shows that there is a concentration of energy at the inertial period during the time intervals when the attenuation fluctuated the most. Energy concentrations at the inertial period are also present in the spectra for the 7 and 17 mab attenuations during the periods when the attenuations vary most (not shown). The wavelet spectrum also shows that there are several intervals when even the 1 mab beam attenuation varies at the inertial period (Figure 11). These results show that changes in the attenuations at all elevations are at least partly due to inertial wave action, but that longer term processes are also important.

The wavelet cross coherence (Torrence and Webster, 1999) measures the degree that two parameters covary as a function of both time and period; as such it is analogous to the classic bivariate coherence (which measures how well two parameters covary at a given period over the entire observation interval). The cross coherence may be high even when the wavelet power spectra for the individual parameters are low; this indicates that a relationship exists between the parameters even when the parameters do not vary too much. The wavelet phase angle is also analogous to that in classical time series analysis, but it determines the phase angle as a function of both time and period. The wavelet cross coherences show that at the inertial period the velocity components at the various elevations are strongly covaring at virtually all times during the deployment (not shown). The phase angle at the inertial period between the cross-shore and alongshore components at each elevation is 90°, as would be expected since the water motion due to inertial waves is nearly circular. The cross coherences between both the temperatures and the attenuations measured at different elevations are far less consistent. For the temperatures at least, this is because the temperature variations at the lower three elevations are so small. The attenuation variations are larger, but the measurements made at different elevations show relatively little cross coherence at the inertial period. This probably reflects real differences in the behavior of suspended sediment at different elevations. The cross coherence between the 1 and 7 mab attenuations is greatest at periods longer than about 50 h (Figure 12) but there is little cross coherence at the inertial period. In fact the cross coherence is greater at periods shorter than the inertial period. This may indicate that the actual mechanism for causing the changes in bac occurs at periods somewhat shorter than the inertial period, or it may be that – since there is little energy at these shorter periods for either of the attenuations – that the result is unimportant. The variations in the two attenuations at the inertial period are roughly in phase during most of the intervals when the cross coherence is significantly different from zero. The cross coherence between the near bottom (1 and 7 mab) attenuations and the 17 mab attenuations is more focused at the inertial frequency, but the phase angles are less consistent. High cross coherences between the 35 mab and the other attenuations are concentrated at the inertial frequency but the phase angles show no consistency.

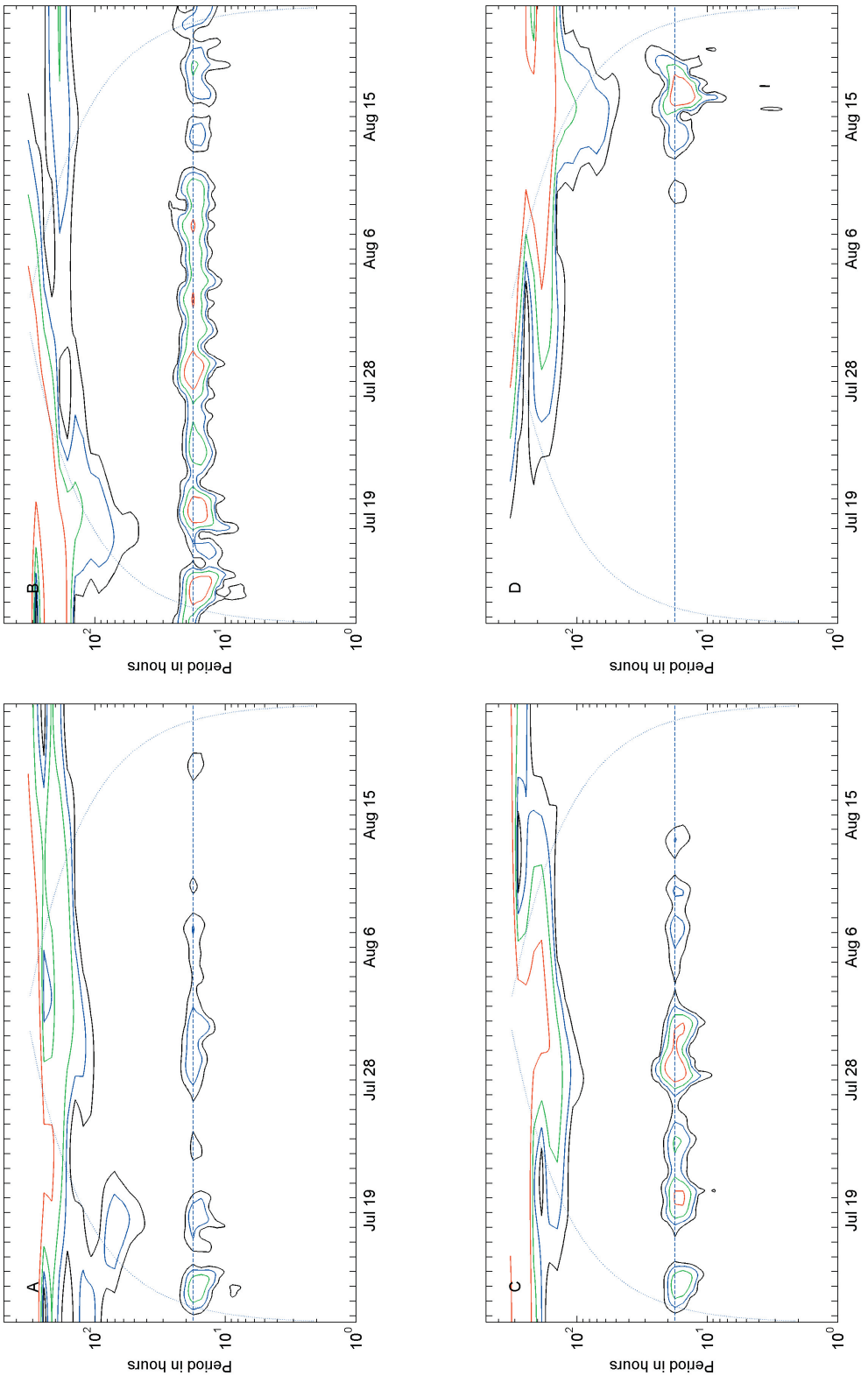

Figure 10. Wavelet power spectra for the parameters measured at 35 mab at M27. The black contour represents the minimum value significantly different from zero at the 95% confidence level. The other contours represent multiples of this value (2 for the blue contour, 4 for the red contour and 8 for the green contour). The horizontal dashed line is the inertial frequency (17.6 h). The curved dotted lines represent the cone of influence where edge effects influence the values of the power spectra. The first tick mark on the horizontal axis is July 12. **A.** Alongshore velocity. **B.** Cross shore velocity. **C.** Temperature. **D.** Attenuation.

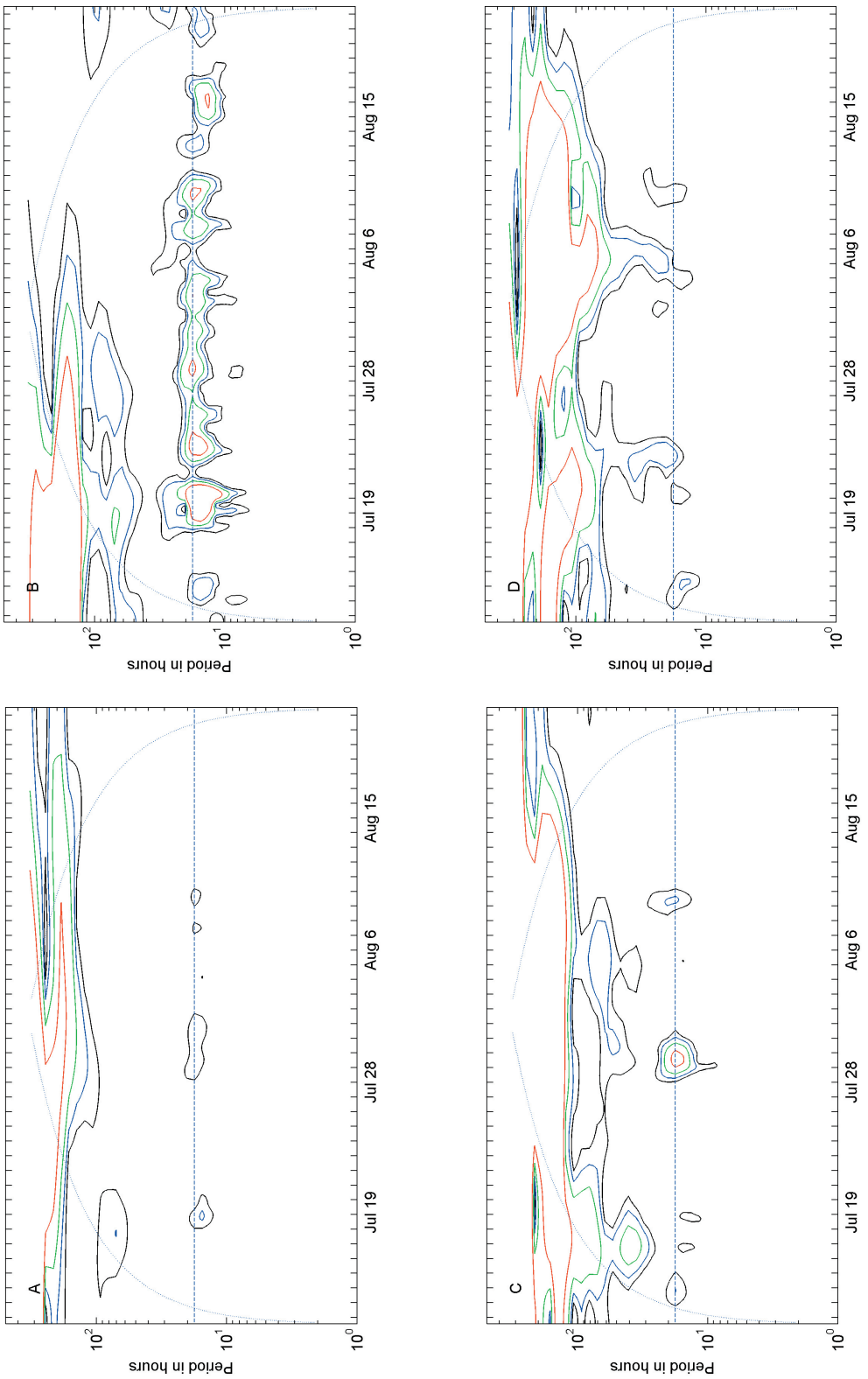

Figure 11. Wavelet power spectra for the parameters measured at 1 mab at M27. The black contour represents the minimum value significantly different from zero at the 95% confidence level. The other contours represent multiples of this value (2 for the blue contour, 4 for the red contour and 8 for the green contour). The horizontal dashed line is the inertial frequency (17.6 h). The curved dotted lines represent the cone of influence where edge effects influence the values of the power spectra. The first tick mark on the horizontal axis is July 12. **A.** Alongshore velocity. **B.** Cross shore velocity. **C.** Temperature. **D.** Attenuation.

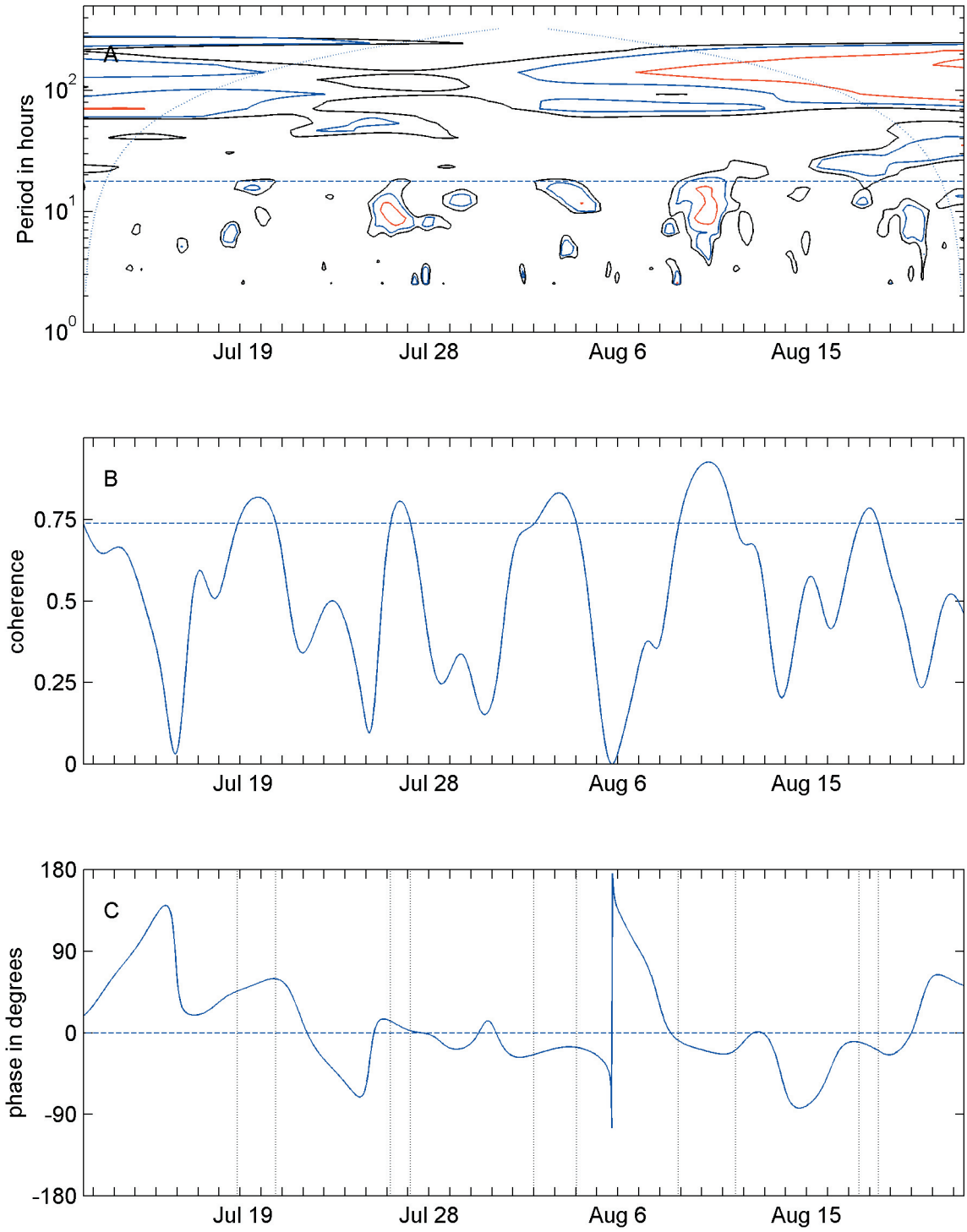

Figure 12. **A.** Wavelet cross coherence for the beam attenuations at 1 and 7 mab at M27. The black contour is the value at which the coherence is significantly different from zero at the 95% confidence level (0.74), the blue contour is 0.85 and the red contour 0.95. The horizontal line is the inertial period (17.6 h). The first tick mark is July 12. The dotted curved lines are the cone of influence. **B.** The cross coherence at the inertial period. The horizontal dashed line is the value above which the coherence is significantly different from zero at the 95% confidence level. **C.** The phase angle. The vertical dotted lines mark the periods where the coherence is significantly different from zero. A negative value means that the 1 mab attenuation lags the 7 mab attenuation.

At 35 mab the cross coherences at the inertial period between the attenuation and the other parameters are significant during most of the deployment, and the phase angle between the attenuation and the temperature is close to zero. Since the vertical profiles show that the 35 mab sensors were usually located above the bnl, the changes in the beam attenuation at 35 mab are most likely due to changes in the depth of the inl caused by the passage of inertial internal waves. Hawley and Muzzi (2003) showed that the depth of the inl moves up and down with the depth of the thermocline, so (since the 35 mab sensors were usually located below the inl) as the depth of the thermocline increases both the temperature and the attenuation at 35 mab increase, while the reverse is true as the thermocline depth decreases. The long-term increase in attenuation after August 12 is most likely due to the increased development of the inl after about August 9 (Figure 2).

Changes in the 35 mab attenuation at the inertial period are also in phase with changes in the direction of the alongshore velocity during most of the deployment (and 90° out of phase with the cross-shore component). Although changes in the current direction might conceivably be the cause of the changes in the bac, there is no other evidence to suggest that this is the case. Maximum alongshore velocities are to the north and maximum cross-shore velocities are onshore, so the peak attenuations occur when the inertial component of the velocity is essentially alongshore to the north. Changes in the 35 mab temperature are also essentially in phase with the alongshore component, but this appears to be merely coincidence; at other locations the relationship could be different.

The changes in the attenuation seen in both the vertical profiles and the time series measurements show that the amount of material in suspension in the bnl increases several times during the deployment and that these increases are related to the inertial waves, but the source of the additional material is unclear. Resuspension events are usually identified by simultaneous increases in bottom attenuation and an increase in either the bottom current velocity or surface waves, but no such increases are apparent at this station. In fact the largest increases in bottom attenuation occur when the current speeds are near their minimum value. Advective episodes are usually identified by a simultaneous change in both attenuation and some other property of the water (such as temperature) or by a change in current direction. At 1 mab the cross coherence between the attenuation and both the speed and the temperature are almost never significant, but the cross coherence between the attenuation and the cross shore velocity is significant during several intervals. The intervals of high cross coherence tend to be centered at periods equal to or slightly less than the inertial period. During the intervals when the cross coherence at the inertial period is significant, the phase angle between the attenuation and the cross shore velocity varies, but during the three intervals that occur when the inertial motions are most pronounced (July 19-21, August 2-3, and August 9-11), peaks in the cross-shore velocity lag peaks in the attenuations by between 30° and 80° (Table 3). This means that the attenuations peaks occur at times when the cross shore velocity is increasing in the onshore direction. During the other three intervals (which occur when the currents are mostly alongshore) the attenuation peaks occur when the cross shore velocity is either directed onshore but has passed its maximum value and is slowing down (July 13-15), or the cross shore velocity is near its maximum and directed offshore (July 25 and August 22). However the attenuation energy during these last two intervals is not significant, so during all of the periods when the energy in both the attenuation and the cross shore velocity are significant, and the cross coherence between the two is also significant, the inertial component of the velocity is onshore. Similar relationships are observed at both 7 mab and 17 mab. At 17 mab, the phase relationships are even more consistent than at 1 mab, and show that the attenuation peaks always occur just after the cross shore velocity starts to increase in an onshore direction. This is not too significant, however, since if the sensor were at another depth the phase relationship would probably be different.

The phase angle between the 1 and the 7 mab attenuations (Figure 12) is close to zero during intervals of high cross coherence so changes in the attenuations near the bottom are not greatly different. The situation is quite different when the 1 and 17 mab attenuations are compared. The phase angles during the intervals of high coherence vary markedly, showing that the two attenuations are either essentially out of phase, or essentially in phase. The phase angles between the 7 and 17 mab attenuations are very similar to those between the 1 and 17 mab observations. The intervals when the 17 mab attenuations are essentially out of phase with the bottom attenuations identify times when the thickness of the bnl varies but the total amount of material suspended

Table 3. Periods of high wavelet cross coherence between the 1 mab attenuation and the cross shore velocity at M27, the wavelet energies of the 1 mab attenuation and the 1 mab cross shore velocity, and the phase angle between the two parameters. X indicates that the value is significantly different from zero. A negative phase angle means that the first parameter lags the second. The second, fourth, and fifth episodes occurred during upwelling events.

Dates	Cross Coherence between 1 mab bac and 1 mab cross shore velocity	Energy of 1 mab Bac	Energy of 1 mab cross shore velocity	Phase angle between 1 mab bac and 1 mab cross shore velocity
July 13-15	X	X	X	60-90°
July 19-21	X	X	X	-80°
July 25	X	-	X	170°
August 2-3	X	X	X	-30°
August 9-11	X	X	X	-30°
August 22	X	-	X	-170°

remains relatively constant. In this case as the thickness of the bnl increases past the 17 m level the attenuation at this level would increase, while the attenuation nearer the bottom would decrease as suspended material is advected upward. Times when changes in the 17 and the bottom attenuations are in phase case are intervals when the thickness of the bnl increases as new material is introduced and thins as this material then settles out of the water column. These intervals occur during upwellings, so the increased onshore velocities during these intervals either somehow initiated local resuspension or advected more turbid water from farther offshore.

Although inertial waves are present at M24, the effects of upwelling and downwellings are the most important process affecting the bac. The bac at 1 mab reaches its highest values during the upwellings on July 17-20 and July 31-August 4 (Figure 3). This reflects the increase in attenuation that occurs when the thermocline moves inshore of the station during upwelling events. Lee and Hawley (1998) previously noted this relationship and determined that the increase in turbidity was considerably greater than that in the bnl further offshore. This is not true during this deployment; the maximum near bottom attenuations observed at M24 are considerably less than those at M27 or in the profiles made at the 45 m station, and can be explained as the result of the bnl being present at the station during upwelling events. The effects of inertial waves are also evident - the cross coherences at the inertial period between the near bottom attenuations and the temperatures are significant and out of phase during a large part of the deployment – but the inertial waves merely modulate the increased bac due to the upwelling events.

At M19 the currents are due almost entirely to inertial wave action, but the attenuations show much less relationship to the activity of these waves than they do at M27. The most noticeable feature of the attenuations is the increase in thickness of the bnl during the deployment from less than 7 m to over 35 m (Figure 8). The wavelet power spectra of the currents show that the energy at the inertial period is significantly different from zero almost continuously at all elevations, but the bac energy is significantly different from zero only during those intervals when the top of the bnl moved up and down past the sensors (July 12-17 and 18-22 at 7 mab, July 22-26 and July 28-August 2 at 17 mab, August 5-August 11 and August 14-16 at 35 mab). The energy of the 1 mab attenuation is never significantly different from zero. Due to the small variations in the water temperatures at the four lower elevations, the wavelet energy at the inertial frequency is seldom significantly different from zero, but at 65 mab the wavelet energy at the inertial frequency for the temperature is significantly different from zero during most of July.

The cross coherences at M19 show that the currents at all of the elevations are essentially in phase, but there is little coherence between either the temperatures or the attenuations at the different elevations, nor do the

cross coherences between the attenuation and the currents at the same depth show any consistent relationships. Although the vertical profiles clearly show that the amount of material in the bnl varies with time, the available data do not indicate a possible mechanism. Local resuspension seems unlikely given the low current speeds and the lack of energy in the bottom attenuation at the inertial period, and the small amount of net transport during the deployment (net bottom transport during the deployment is less than 10 km towards shore) argues against advective transport. The transport direction is onshore during the time when the thickness of the bnl was increasing, so if the increase in thickness is due to advection, the source of the more turbid water must be even farther offshore.

4. DISCUSSION

The occurrence of high attenuations during times when no obvious forcing occurs have been noted by numerous researchers in a variety of environments. Although no actual observations of bottom resuspension by internal waves were observed in this study, the data strongly suggest that such episodes do occur and that these episodes are in large part responsible for maintaining the bnl. The observations at M27 are similar to observations reported by Puig et al. (2001) from the Mediterranean Sea, who described the resuspension of bottom sediments by internal waves at a site located in 60 m of water. They found a strong correspondence between increases in suspended material near the bottom and changes in the near-bottom temperature (decreased), salinity (increased), and current direction (changed to onshore) at a period (17 h) slightly shorter than the inertial period (18.5 h). These correlations are similar to those observed at M27 during upwelling events (although no significant changes in temperature occurred, increases in near-bottom suspended sediment concentration were in phase with increased onshore velocities), so it is quite possible that bottom resuspension by internal waves also occurs in Lake Michigan. However the Brunt-Väisälä frequency and the bottom slope at M27 only allow waves with periods of about one hour or less to be transmitted upslope during the deployment (Cacchione and Drake, 1986), so any resuspension must be due to waves with periods much less than the inertial period. Observations of the resuspension of bottom material by short period internal waves (internal solitons) have been described by Bogucki et al. (1997) and Johnson et al. (2001) on the California continental shelf, but the one hour sampling interval makes it impossible to identify such waves in the data presented here. The bottom slope at M19 is much less than at M27 and M24, so near-inertial waves could cause local resuspension, but there is no evidence of their existence.

It is also clear that while inertial wave action may (either directly or indirectly) cause local resuspension, resuspension does not occur all of the time. If resuspension does occur at M27, it appears that the appropriate conditions are related to the occurrence of upwelling events, which temporarily diminish the magnitude of the alongshore currents (Rao and Murthy, 2001). This allows the onshore movement of bottom water, which may then in turn generate the internal waves responsible for the resuspension of the bottom material. Hawley and Muzzi (2003) also observed an increase in the thickness of the bnl during two upwelling events at a station close to M27, but were unable to identify the process responsible for the increase. At M19, where inertial wave action predominated throughout the deployment, brief local resuspension events may occur more frequently (although none were observed) and could explain the increase in thickness of the bnl during the deployment.

The location of M24 just offshore of the area where the thermocline intersects the lake bottom would seem to make it a likely site to observe resuspension by breaking internal waves. Although increased bottom attenuations were observed during upwellings and the attenuations did vary at the inertial period, the maximum attenuations were no higher than those observed in the bnl farther offshore. Increases in the bottom attenuation are correlated with decreased temperatures, so it likely that the increases were due to simple advection of more turbid bottom water from farther offshore without requiring local resuspension. However Lee and Hawley (1998) reported greatly increased attenuations at the same station during upwellings in September and October, so local resuspension may have occurred during the stronger upwellings that occurred later in the year.

If resuspension is the cause of the bnl then the material suspended in the water column should be similar to that on the bottom, but only a few studies have analyzed the chemical and mineralogic composition of material suspended

in the bnl in the Great Lakes. Eadie et al. (1984) and Robbins and Eadie (1991) both found that the chemical composition of material collected in near-bottom sediment traps closely resembled that collected from the lake bottom, but Harrsch and Rea (1982) and Mudroch and Mudroch (1992) found that suspended sediment collected from water samples contained a much higher abundance of biologic material than did the surface sediments. This discrepancy may be at least partly due to the fact that water samples and sediment traps preferentially collect different types of material. Sediment traps tend to collect larger, more quickly settling particles, while material collected from water samples is biased toward smaller, more slowly settling material. Radiometric data (Robbins and Eadie, 1991) also shows that near-bottom trap material is derived primarily from bottom sediments, but the composition of material in the bnl undoubtedly varies with time and location.

A variety of inls with different origins have been described in the literature. Puig and Palanques (1999) described shelf inls, shelf-break inls, and slope inls in the Mediterranean Sea. The inl described here is similar to the shelf inl of Puig and Palanques (which they showed also occurred in deeper water seaward of the edge of the continental shelf), and is also similar to the inl described by Palanques and Biscaye (1992) on the continental shelf off of the eastern coast of the United States. Both of these papers describe a nepheloid layer occurring near the base of the thermocline (which is the location of the inl described here) and ascribe its origin to the accumulation of biological material. Gardner et al. (2001) described the same layer as occurring at the base of the mixed layer on the Atlantic continental shelf, and showed that the peak in bac occurred several meters above the maximum values of fluoresence and chlorophyll measurements. Although no measurements of chlorophyll were made during this study, fluoresence measurements made during the vertical profiles show a rapid increase in the inl with a maximum value 10-20 m below the peak in bac. Barbiero and Tuchman (2001) have ascribed these increases in fluorescence to the presence of biological material, so the particles in the inl are probably mostly biological in origin. Harrsch and Rea (1982) also found high concentrations of biological material in the inl.

Profiles made during the winter (Hawley and Lee, 1999) and spring (Hawley, unpublished data) show that nepheloid layers occur intermittently during the unstratified period, but as the thermal bar moves offshore and the lake becomes stratified, a persistent bnl becomes increasingly well-developed. By the beginning of this deployment, an inl had also become established at the base of the thermocline. Both the thickness of the bnl and the amount of material in suspension varied during the summer, but the layer was always present at both M27 and M19, and was present at M24 whenever the water was stratified. Later in the year, as the water started to cool and vertical mixing became more intense, the nepheloid layers disappeared. The inl was gone by the end of September (Lee and Hawley, 1998), but the bnl persisted until late October at M24 and later than that at the deeper stations (Lee and Hawley, 1998, Hawley unpublished data). Thus the development and decay of the nepheloid layers follows the thermal cycle of the lakes to a large degree, although storms during the unstratified period create a temporary bnl.

5. CONCLUSIONS

Although these conclusions should be regarded as preliminary, the observations clearly show that inertial internal waves have a significant effect on the vertical distribution of suspended material in Lake Michigan during the stratified period. Although the precise mechanisms are still unknown, both the thickness and the distribution of suspended material within the bnl vary with the same period as the inertial waves in the lake. Although the observations show no direct evidence of local bottom resuspension due to internal wave activity, the data strongly suggest that such episodes do occur. Unfortunately the short length of the deployment and the long sample interval make it impossible to determine if either near-inertial waves or short period internal solitons occurred. When the changes in bac due to inertial internal waves are compared to those due to upwelling and downwelling events, it is clear that the longer-term processes are at least as important in determining the total amount of suspended sediment, and are also responsible for creating the conditions where inertial waves can cause (either directly or indirectly) sediment resuspension. Unfortunately the vertical profiles were all taken at least 1 day apart, so it cannot be determined if the total amount of suspended sediment varied over a single inertial cycle. More extensive measurements (including both vertical profiles made several times during a single inertial period and continuous time series measurements) will be needed before the effect of internal waves on the bnl will be fully understood.

The vertical movement of the inl occurs in response to changes in thermocline depth due to both upwelling and downwelling events, and to inertial wave motion. The inl in the lake is similar to the shelf inl described in the oceans and is probably due to a concentration of biological material near the base of the thermocline.

The use of wavelets has considerable advantages over more traditional time series techniques since wavelets allow the data to be examined as a function of both time and period (or frequency). Although the analyses were not able to determine whether or not resuspension due to near-inertial waves occurred, the wavelet analyses were able to identify periods within the deployment where changes in bac showed a consistent relationship to changes in other parameters. As in more traditional analyses, the fact that data were only collected at specified elevations makes the analysis more complex since only intervals when changes occurred at those specific elevations can be evaluated. Use of in situ vertical profiler would allow data to be collected throughout the water column at regular intervals. Such data would almost certainly be easier to analyze and would allow the resolution of some of the questions that remain unanswered by this study.

6. REFERENCES

Baker, J. E., and S.J. Eisenreich. PCBs and PAHs as tracers of particulate dynamics in large lakes. *Journal of Great Lakes Research* 15: 84-103 (1989).

Barbiero, R.P., and M.L. Tuchman. Results from the U.S. EPA's biological open water surveillance program of the Laurentian Great Lakes: II. Deep chlorophyll maximum. *Journal of Great Lakes Research* 27: 155-166 (2001).

Bogucki, D., T. Dickey, and L.G. Redekopp. Sediment resuspension and mixing by resonantly generated internal solitary waves. *Journal of Physical Oceanography* 27: 1181-1196 (1997).

Boyce, F.M., M.A. Donelan, P.F. Hamblin, C.R. Murthy, and T.J. Simons. Thermal structure and circulation in the Great Lakes. *Atmosphere-Ocean* 27: 607-642 (1989).

Cacchione, D.A., and D.E. Drake. Nepheloid layers and internal waves over continental shelves and slopes. *Geo-Marine Letters* 6: 147-152 (1986).

Chambers, R.L., and B.J. Eadie. Nepheloid and suspended particulate matter in southeastern Lake Michigan. *Sedimentology* 28: 439-447 (1981).

Eadie, B.J., R.L. Chambers, W.S. Gardner, and G.L. Bell. Sediment trap studies in Lake Michigan: resuspension and chemical fluxes in the southern basin. *Journal of Great Lakes Research* 10: 307-321 (1984).

Gardner, W.D., J.C. Blakey, I.D. Walsh, M.J. Richardson, S. Pegau, J.R.V. Zaneveld, C. Roesler, M.C. Gregg, J.A. MacKinnon, H.M. Sosik, and A.J. Williams III. Optics, particles, stratification, and storms on the New England continental shelf. *Journal of Geophysical Research* 106: 9473-9497 (2001).

Halfman, B.M., and T.C. Johnson. Surface and benthic nepheloid layers in the western arm of Lake Superior, 1983. *Journal of Great Lakes Research* 15: 15-25 (1989).

Harrsch, E.C., and D.K. Rea. Composition and distribution of suspended sediments in Lake Michigan during summer stratification. *Environmental Geology* 4: 87-98 (1982).

Hawley, N. and C-H. Lee. Sediment resuspension and transport in Lake Michigan during the unstratified period. *Sedimentology* 46: 791-805 (1999).

Hawley, N., and B.M. Lesht. Does local resuspension maintain the benthic boundary layer in Lake Michigan? *Journal of Sedimentary Research* A65: 69-76 (1995).

Hawley, N., and C.R. Murthy. The response of the benthic nepheloid layer to a downwelling even. *Journal of Great Lakes Research* 21: 641-651 (1995).

Hawley, N., and R.W. Muzzi. Observations of nepheloid layers made with an autonomous vertical profiler. *Journal of Great Lakes Research* 29: 124-133 (2003).

Hawley, N., and J.E. Zyren. Transparency calibration for Lake St. Clair and Lake Michigan. *Journal of Great Lakes Research* 16: 113-120 (1990).

Jenkins, G.M., and D.G. Watts. Spectral analysis and its applications. Holden-Day, San Francisco, CA., 525 pp. (1969).

Johnson, D.R., A. Weidemann, and W.S. Pegau. Internal tidal bores and bottom nepheloid layers. *Continental Shelf Research* 21: 1473-1484 (2001).

Lee, C-H., and N. Hawley. The response of suspended particulate material to upwelling and downwelling events in southern Lake Michigan. *Journal of Sedimentary Research* 68: 819-831 (1998).

Li, M. Z., and C.L. Amos. SEDTRANS96: the upgraded and better calibrated sediment-transport model for continental shelves. *Computers and Geosciences* 27: 619-645 (2001).

Liu, P.C., and G.S. Miller. Wavelet transform and ocean current data analysis. *Journal of Atmospheric and Oceanic Technology* 13: 1090-1099 (1996).

Meyers, S.D., B.G. Kelly, and J.J. O'Brien. An introduction to wavelet analysis in oceanography and meteorology: with applications to the dispersion of Yanai waves. *Monthly Weather Review* 121: 2858-2866 (1993).

McCave, I.N. Local and global aspects of the bottom nepheloid layer in the world ocean. *Netherlands Journal of Sea Research* 20: 167-181 (1986).

Mortimer, C.H. Inertial Motion and Related Internal Waves in Lake Michigan and Lake Ontario as Responses to Impulsive Wind Stresses. Special Report 37, Center for Great Lakes Studies, Milwaukee, Wisconsin. 192 pp. (1980).

Mudroch, A., and P. Mudroch. Geochemical composition of the nepheloid layer in Lake Ontario. *Journal of Great Lakes Research* 18: 132-153 (1992).

Murthy, C.R., and D.S. Dunbar. Structure of the coastal boundary layer of the Great Lakes. *Journal of Physical Oceanography* 11: 1567-1577 (1981).

Palanques, A., and P.E. Biscaye. Patterns and control of the suspended matter distribution over the shelf and upper slope south of New England. *Continental Shelf Research* 12: 577-600 (1992).

Puig, P., and A. Palanques. Nepheloid structure and hydrographic control on the Barcelona continental margin, northwestern Mediterranean. *Marine Geology* 149: 39-54 (1999).

Puig, P., A. Palanques, and J. Guillén. Near-bottom suspended sediment variability caused by storms and near-inertial internal waves on the Ebro mid continental shelf (NW Mediterranean). *Marine Geology* 178: 81-93 (2001).

Rao, Y.R., and C.R. Murthy. Nearshore currents and turbulent exchange processes during upwelling and downwelling events in Lake Ontario. *Journal of Geophysical Research* 106: 2667-2678 (2001).

Ribbe, J., and P.E. Holloway. A model of suspended sediment transport by internal tides. *Continental Shelf Research* 21: 395-422 (2001).

Robbins, J.A., and B.J. Eadie. Seasonal cycling of trace elements ^{137}Cs, ^{7}Be, and $^{239+240}Pu$ in Lake Michigan. *Journal of Geophysical Research* 96: 17,081-17,104 (1991).

Rosa, F. Sedimentation and sediment resuspension in Lake Ontario. *Journal of Great Lakes Research* 11: 13-25 (1985).

Sandilands, R.G., and A. Mudroch. A. Nepheloid layer in Lake Ontario. *Journal of Great Lakes Research* 9: 190-200 (1983).

Schwab, D.J., J.R. Bennett, and P.C. Liu. Application of a simple numerical wave prediction model to Lake Erie. *Journal of Geophysical Research* 89: 3586-3592 (1981).

Sly, P.G. Sedimentary processes in lakes, In: *Sediment Transport and Depositional Processes* (Ed by K. Pye). Blackwell Scientific Publications, Oxford, England, 157-191 (1994).

Torrence, C., and G.P. Compo. A practical guide to wavelet analysis. *Bulletin of the American Meteorological Society* 79: 61-78 (1998).

Torrence, C., and P.J. Webster. Interdecadal changes in the ENSO-monsoon system. *Journal of Climate* 12: 2679-2690 (1999).

Wang, B. J., D.J. Bogucki, and L.G. Redekopp. Internal solitary waves in a structured thermocline with implications for resuspension and the formation of thin particle layers. *Journal of Geophysical Research* 106: 9565-9585 (2001).

Weng, H.Y., and K.M. Lau. Wavelets, period doubling and time-frequency localization with application to organization of convection over the tropical western Pacific. *Journal of Atmospheric Research* 51: 2523-2541 (1994).